Catalysis Today 174 (2011) 25–30

Contents lists available at ScienceDirect

Catalysis Today

journal homepage: www.elsevier.com/locate/cattod

Hydrogen sulfide oxidation on R_E(R_E = Sm, Y, La)–V–Sb catalysts: Effects of R_E size and electronegativity

Kuo-Tseng Li*, Chen-Hwa Huang

Department of Chemical Engineering, Tunghai University, No. 181, Section 3, Taichung Port Road, Taichung, Taiwan, ROC

ARTICLE INFO

Article history:
Received 18 October 2010
Received in revised form 6 March 2011
Accepted 26 March 2011
Available online 24 May 2011

Keywords:
Hydrogen sulfide oxidation
Sulfur selectivity and yield
Rare earth orthovanadates
Antimony oxide
Site isolation
Electronegativity

ABSTRACT

Three R_E–V–Sb (R_E was Sm, Y, and La) mixed-oxide catalysts were prepared for catalyzing the selective oxidation of hydrogen sulfide to sulfur. The multiphase R_E–V–Sb catalysts were characterized by TPR, XRD, SEM and BET techniques. Synergistic phenomena in sulfur yield were observed with the solid-state reaction between R_EVO_4 and α-Sb_2O_4 (antimony oxide/R_EVO_4 weight ratio = 1/3), which was ascribed to the formation of $SbVO_4$ species. Under identical reaction conditions, areal reaction rate decreased in the following order: Sm–V–Sb > La–V–Sb ∼ $LaVO_4$ > Y–V–Sb > $SmVO_4$ > YVO_4. All R_E–V–Sb catalysts exhibited 100% sulfur yield in a certain temperature range. The temperature window width for 100% sulfur yield decreased in the following order: La > Sm > Y, which was the same as the order of decreasing ionic radius (La > Sm > Y) and the order of increasing R_E electronegativity (La < Sm < Y). The selectivity difference was explained in terms of active site isolation and product desorption effects. The rare earth cation size effect observed here for H_2S oxidation to elemental sulfur was similar to the alkali cation size effect reported for the hydrocarbon oxidation.

1. Introduction

Hydrogen sulfide is a by-product of many industrial operations, such as hydrodesulfurization of crude oil, natural gas and coal [1]. It is usually converted to elemental sulfur in sulfur-recovery plants or so-called Claus plants. Due to thermodynamic limitation, the sulfur recovery offered by a Claus process is limited in practice to about 97%. About 1% of H_2S remains in the off-gas of a Claus plant [2]. Because of the strict air pollution regulations, a variety of Claus tail gas treatment (TGT) processes have been developed to increase the total sulfur-recovery efficiency [3]. Dry type Claus TGT processes have been developed which comprise a step of recovering elemental sulfur from Claus tail gas by selective oxidation of hydrogen sulfide using the following catalytic reaction [4,5]:

$$H_2S + 1/2O_2 \rightarrow \left(\frac{1}{n}\right) S_n + H_2O \quad (n = 6 \rightarrow 8) \tag{1}$$

The method of partial catalytic oxidation of hydrogen sulfide to elemental sulfur, is also being increasing used in industry for treating H_2S—containing natural gases. This method does not require preliminary treatment of the gases and concentration of hydrogen sulfide, is more promising than the Claus method [6].

In addition to the production of sulfur in Eq. (1), sulfur dioxide can also be generated simultaneously due to side reactions (e.g., $(1/n)S_n + O_2 \rightarrow SO_2$). Therefore, a good hydrogen sulfide oxidation catalyst should be able to maximize the sulfur yield and to minimize the sulfur dioxide generation.

Rare earth element is the general name given to the 15 lanthanide elements together with Sc and Y elements. Characteristics of the rare earth elements lie in their relatively large ionic radii (1–1.17 Å) and small electronegativities [7]. Earlier work from our laboratory showed that several rare earth orthovanadates had better sulfur yield than vanadium oxide alone for the selective oxidation of hydrogen sulfide [8]. Sulfur yields of these rare earth orthovanadates were not high enough and their sulfur selectivities were sensitive to temperature change. It is therefore desired to develop catalysts with a higher sulfur yield and with a reasonable range of operation temperature, which can easily withstand inadvertent plant upsets.

In this work, selective oxidation of hydrogen sulfide to sulfur was carried out over three R_EVO_4 (R_E was Sm, Y, and La) with antimony oxide as an additive. We observed that the addition of antimony oxide significantly improved the sulfur yield of these rare earth orthovanadates, and all of the R_E–V–Sb catalysts exhibited 100% sulfur yield in certain temperature ranges. Temperature window width for 100% sulfur yield decreased in the following order: La > Sm > Y, which was the same as the order of decreasing ionic radius (La > Sm > Y).

* Corresponding author. Fax: +886 4 23590009.
E-mail address: ktli@thu.edu.tw (K.-T. Li).

0920-5861/$ – see front matter © 2011 Elsevier B.V. All rights reserved.
doi:10.1016/j.cattod.2011.03.070

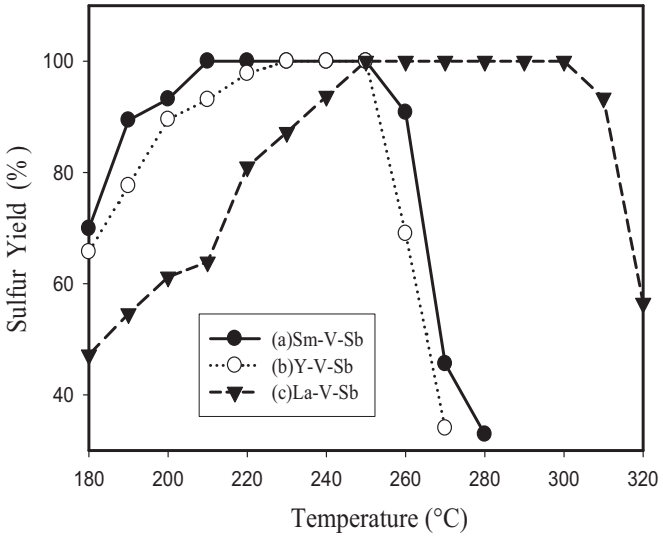

Fig. 1. Effect of reaction temperature on sulfur yield for Sm–V–Sb (curve a), Y–V–Sb (curve b), and La–V–Sb (curve c) catalysts.

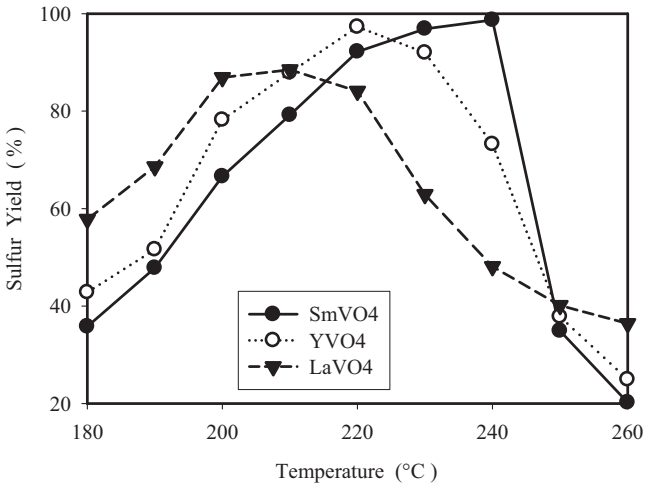

Fig. 2. Relationships between sulfur yield and reaction temperature for $SmVO_4$, YVO_4, and $LaVO_4$.

2. Experimental

2.1. Catalyst preparation and characterization

R_E–V–Sb catalysts were prepared by mechanically mixing α-Sb_2O_4 with R_EVO_4 (α-Sb_2O_4/R_EVO_4 weight ratio = 1/3) in *n*-pentane, followed by evaporation in vacuum (at 60 °C), drying (at 80 °C for 12 h), and calcination (at 600 °C for 144 h). R_EVO_4 was prepared by citrate method [9,10]. The starting materials were Sm_2O_3 (Strem), Y_2O_3 (Strem), La_2O_3 (ACROS Organics, Belgium) and NH_4VO_3 (Showa Chemicals, Tokyo). The main preparation steps were reported before [8]. Crystal structures of the catalysts were analyzed by X-ray diffraction crystallography on a Shimadzu XRD-6000 diffractometer with Cu Kα radiation. Catalyst surface areas were determined by nitrogen adsorption with a Micromeritics BET surface area analyzer (Model ASAP2020). Catalyst reducibility was studied with temperature-programmed reduction (TPR) method, which was conducted using 0.15 g of catalyst in a stream of 10% hydrogen in argon and with a heating rate of 10 °C/min. The microscopic aspect of the catalysts was examined under a scanning electron microscope (TOPCON ABT-32).

2.2. Reaction studies

Selective oxidation of hydrogen sulfide to elemental sulfur was carried out in a continuous flow reactor containing 0.2 g of catalyst. Before the catalytic studies, catalysts were pretreated in an environment of 9 vol% hydrogen sulfide at 250 °C for 8 h. After the pretreatment stage, the reactor temperature was decreased to 180 °C and a gaseous feed consisting of 1 vol% hydrogen sulfide, 5 vol% oxygen and 94 vol% nitrogen was introduced into the reactor. The gaseous feed flow rate was 200 ml/min. The experimental data were taken 14 h after the catalyst pre-treatment stage. Experimental results confirmed the good reproducibility was achieved when the same reaction temperature was used, which indicated that the reaction reached the steady state during the tests of catalytic properties.

The gas products were dried and analyzed by a gas chromatograph using a 9-m-long Porapak Q column. Reaction conversion was defined as (moles of hydrogen sulfide reacted)/(moles of hydrogen sulfide fed) × 100%. Sulfur selectivity was calculated as (moles of hydrogen sulfide reacted-moles of sulfur dioxide produced)/(moles of hydrogen sulfide reacted) × 100%. Sulfur yield was defined as conversion times selectivity.

3. Results and discussion

3.1. Oxidation of hydrogen sulfide

Figs. 1 and 2 present the relationships between sulfur yield and reaction temperature for R_E–V–Sb catalysts and for R_EVO_4 catalysts, respectively. The curves in Figs. 1 and 2 exhibit a volanco shape with a maximum sulfur yield because conversion increased with temperature while selectivity decreased with temperature. In certain temperature ranges, the maximum sulfur yield reached 100% for all R_E–V–Sb catalysts. The width of temperature window for 100% sulfur yield were 50 °C (in the temperature range of 250–300 °C), 30 °C (in the temperature range of 210–240 °C), and 20 °C (in the temperature range of 230–250 °C) for La–V–Sb, Sm–V–Sb, and Y–V–Sb catalysts, respectively. That is, the temperature window width for 100% sulfur yield decreased in the following order: La–V–Sb > Sm–V–Sb > Y–V–Sb.

For R_EVO_4 alone, the maximum sulfur yields obtained for $LaVO_4$, $SmVO_4$, and YVO_4 were 88.5% (at 210 °C), 98.7% (at 240 °C), and 97.3% (at 220 °C), respectively (shown in Fig. 2). For R_EVO_4 alone, the R_E radius size might change the extent of crystal lattice distortion and resulted in the differences in performances.

In order to minimize the emissions of both H_2S and SO_2, the maximum sulfur yield is the most important criterion for evaluating catalyst performance in the selective oxidation of hydrogen sulfide because sulfur yield = H_2S conversion × sulfur selectivity. Hence, the results in Figs. 1 and 2 indicate that the catalytic performances of R_E–V–Sb samples were superior to those of R_EVO_4 alone, and R_E–V–Sb catalysts exhibited synergistic behavior in the catalytic performances for hydrogen sulfide oxidation.

The oxidation of H_2S may proceed as a sequential oxidation ($H_2S \rightarrow S \rightarrow SO_2$). The decrease of sulfur yield at the higher temperature range (shown in Figs. 1 and 2) suggest that the second reaction step ($S \rightarrow SO_2$) has greater activation energy than the first reaction step ($H_2S \rightarrow S$). In the lower temperature range, the second step reaction was not significant and the only product obtained was elemental sulfur. In the higher temperature range, the second step reaction became more significant and its rate increased rapidly with increasing temperature. Therefore, more sulfur was converted to sulfur dioxide and the sulfur selectivity and sulfur yield decreased with increasing temperature.

Table 1
Catalyst specific surface area before and after H_2S oxidation.

Catalyst	Surface area (m^2/g) (before reaction)	Surface area (m^2/g) (after reaction)
$SmVO_4$ alone	60.9	38.3
Sm–V–Sb	3.1	1.5
YVO_4 alone	70.2	51.5
Y–V–Sb	7.3	5.2
$LaVO_4$ alone	6.3	1.8
La–V–Sb	1.4	1.3
α-Sb_2O_4 alone	0.5	0.4

Table 1 presents catalyst specific surface areas for R_E–V–Sb samples and for R_EVO_4 alone (before and after H_2S oxidation). Surface areas of R_E–V–Sb catalysts were much smaller than those of R_EVO_4 alone, which should be due to the very small surface area of α-Sb_2O_4.

Table 1 indicates that surface areas of the used R_E–V–Sb catalysts decreased in the following order: Y–V–Sb > Sm–V–Sb > La–V–Sb, which is not the same as the order of catalyst activity. Therefore, surface area alone is not responsible for the catalytic activity difference.

Based on the H_2S conversion data in Table 2 and the surface area data of used catalyst (shown in Table 1), specific catalytic activity ($-r_{H_2S}$) was calculated via the following equation:

$$-r_{H_2S} = \left(\frac{\text{gas volumetric flow rate} \times H_2S \text{ volume fraction}}{\text{gas molar volume}}\right) \times H_2S \text{ conversion/catalyst surface area}$$

Calculation results are shown in Table 2. Under identical reaction conditions, areal reaction rate decreased in the following order: Sm–V–Sb > La–V–Sb ~ $LaVO_4$ > Y–V–Sb > $SmVO_4$ > YVO_4. That is, the addition of Sb into $SmVO_4$ and YVO_4 dramatically increased their specific catalytic activity, but the addition of Sb into $LaVO_4$ had little promoting effect on its specific catalytic activity. The promoting effect on specific catalytic activity is most profound for Sm–V–Sb.

For hydrocarbon oxidation, it is known that vicinal V moieties would lead to undesirable overoxidation of the hydrocarbons and result in waste formation [11]. It is therefore necessary to add additional element to isolate the active phase in order to achieve the desirable selectivity (site isolation concept). In rare earth orthovanadates, the bulk VO vanadate ions are isolated (no bridging V–O–V bonds) and the four-coordinated vanadate ions are charge balance by cations R_E^{3+}. The ionic radii of Sm^{3+}, Y^{3+}, and La^{3+} are 0.96 Å, 0.89 Å, and 1.03 Å, respectively [12]. Based on the site isolation hypothesis, the site isolation capability of the three rare earth elements should decrease in the following order La > Sm > Y, which resulted in the following order of sulfur selectivity La–V–Sb > Sm–V–Sb > Y–V–Sb, as shown in Fig. 1.

Electronic effect can also affect sulfur selectivity of R_E–V–Sb catalysts. Elemental sulfur vapor has several different molecular forms (S_2, S_3, …, S_8) [13] and exist as rings (cyclic allotropes such as S_6, S_7, S_8) and chains. Sulfur rings have fully paired electrons and sulfur chains have unpaired electrons at each end [14,15]. The easier desorption of elemental sulfur from the catalyst surface will prevent overoxidation of sulfur to sulfur dioxide. R_E electronegativities should affect the catalytic performances of R_E–V–Sb catalysts for selective oxidation of hydrogen sulfide to elemental sulfur because R_E electronegativity describes the ability of an R_E atom to attract electrons (in sulfur rings or sulfur chains) toward itself. The Pauling electronegativity values of Sm, Y, and La are 1.17, 1.22, and 1.10, respectively [15]. That is, the adsorption strength of elemental sulfur decrease in the following order Y > Sm > La. Therefore, the wider operating temperature range obtained for La–V–Sb (compared to Sm–V–Sb and Y–V–Sb) can be ascribed to its weaker sulfur adsorption strength (i.e., sulfur desorption became easier and therefore less sulfur was overoxidized to sulfur dioxide), which was caused by the lower electronegativity of La.

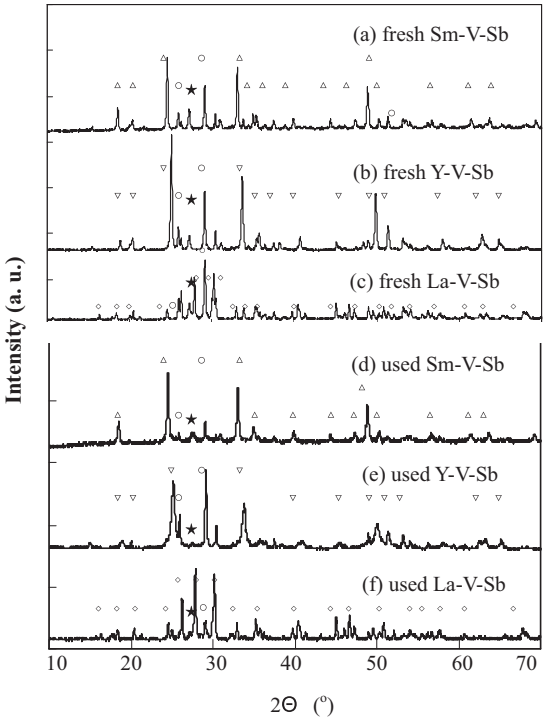

Fig. 3. Powder X-ray diffraction patterns of the fresh catalysts for (a) Sm–V–Sb, (b) Y–V–Sb, (c) La–V–Sb, and used catalysts for (d) Sm–V–Sb, (e) Y–V–Sb, (f) La–V–Sb (*, $SbVO_4$; △, $SmVO_4$; ▽, Y VO_4; ◊, $LaVO_4$; ○, Sb_2O_4).

Our results in Fig. 1 (selectivity increased with increasing cation size) are similar to the alkali cation size effect for hydrocarbon oxidation reported in Martin et al. [16] and Grabowski et al. [17]. Martin et al. studied the effect of alkali metal promotion on vanadium-containing catalysts in the oxidation of substituted toluenes to their corresponding aldehydes. They found that the increasing alkali cation size in the order from Li to Cs leads to an increase in the aldehyde selectivity. Grabowski et al. studied the effect of alkali metal additives to V_2O_5/TiO_2 catalysts on the catalytic performances in oxidative dehydrogenation of propane, and found that the yield and selectivity to propylene increased in the order: RbVTi > KVTi > LiKTi > VTi.

3.2. XRD studies

Fig. 3 shows the powder X-ray diffraction spectra of fresh and used catalysts for (a) Sm–V–Sb, (b) Y–V–Sb, (c) La–V–Sb. Peak positions of the used catalysts are identical to those of fresh catalysts, which indicated that R_E–V–Sb catalyst structure did not change after H_2S oxidation. The XRD results suggest that R_E–V–Sb mixed-oxide (not sulfide) was the active catalytic species for H_2S oxidation. The powder X-ray diffraction patterns of fresh $SmVO_4$, YVO_4, $LaVO_4$, and $SbVO_4$ were also obtained for comparisons. The XRD pattern of $SmVO_4$ (with major peaks at $2\theta = 18.6°$, 24.6°, 33.2°, 49.0°) is similar to that of YVO_4 (with major peaks at $2\theta = 18.9°$, 25.1°, 33.7°, 50°), because they are isomorphous crystals with the body-centered zircon-type tetragonal structure [18]. We also found

Table 2
H_2S conversion and specific catalytic activity ($-r_{H_2S}$; unit = mol of H_2S reacted/m^2 min)) of R_E–V–Sb and R_EVO_4 catalysts for selective oxidation of hydrogen sulfide.[a]

Temperature (°C)	$SmVO_4$	Sm–V–Sb	YVO_4	Y–V–Sb	$LaVO_4$	La–V–Sb
180						
Conv. (%)	35.8	69.9	42.8	65.7	57.8	47.2
$-r_{H_2S} \times 10^6$	3.8	190	3.4	52	130	148
190						
Conv. (%)	47.8	89.4	51.6	77.6	68.6	54.6
$-r_{H_2S} \times 10^6$	5	243	4.1	61	160	171
200						
Conv. (%)	66.6	93.2	78.2	89.5	86.9	61.2
$-r_{H_2S} \times 10^6$	7.1	254	6.2	70	197	192

[a] Reaction conditions: gas flow rate = 200 mL/min with a composition of $H_2S/O_2/N_2$ = 1/5/94 vol% and in the presence of 0.2 g catalyst.

that $LaVO_4$ had a monazite-like monoclinic structure with trace V_2O_5 impurity [12]. The existence of trace V_2O_5 impurity in $LaVO_4$ might result in the higher activity and the lower selectivity of the sample, as shown in Fig. 2. Generally, with increasing ionic radius, R_E^{3+} ions show a strong tendency toward monazite-structured orthovanadate due to its higher oxygen coordination number of 9 as compared with 8 of the zircon-type [19].

For R_E–V–Sb samples, the XRD characteristic peaks in Fig. 3 indicate that the R_EVO_4 phase was accompanied by α-Sb_2O_4 (with a major peak at $2\theta = 29°$), and the formation of new phase was detected. All of the patterns in Fig. 3 have a new peak at $2\theta = 27.4°$ (peak marked with ⋆), indicating the formation of a new compound—$SbVO_4$. Based on the XRD results, the coexistence of $SbVO_4$ and α-Sb_2O_4 in the R_E–V–Sb catalysts might also contribute to the increase of sulfur yield, as reported in Fig. 1. For H_2S oxidation, it is known that $SbVO_4$ had better catalytic performances than V_2O_5 and α-Sb_2O_4 [20]. But R_E–V–Sb catalysts were much less sensitive to temperature change than V–Sb catalyst, and R_E–V–Sb catalysts had a much wider operating temperature range than V–Sb catalyst. That is, R_E improved sulfur selectivity and thermal stability. The sulfur selectivity improvement with Sb addition might be due to the decrease of vanadium oxidation state (i.e., the formation of $VSbO_4$), the better isolation of the active sites, and the decrease of the extent of surface reduction [21–23].

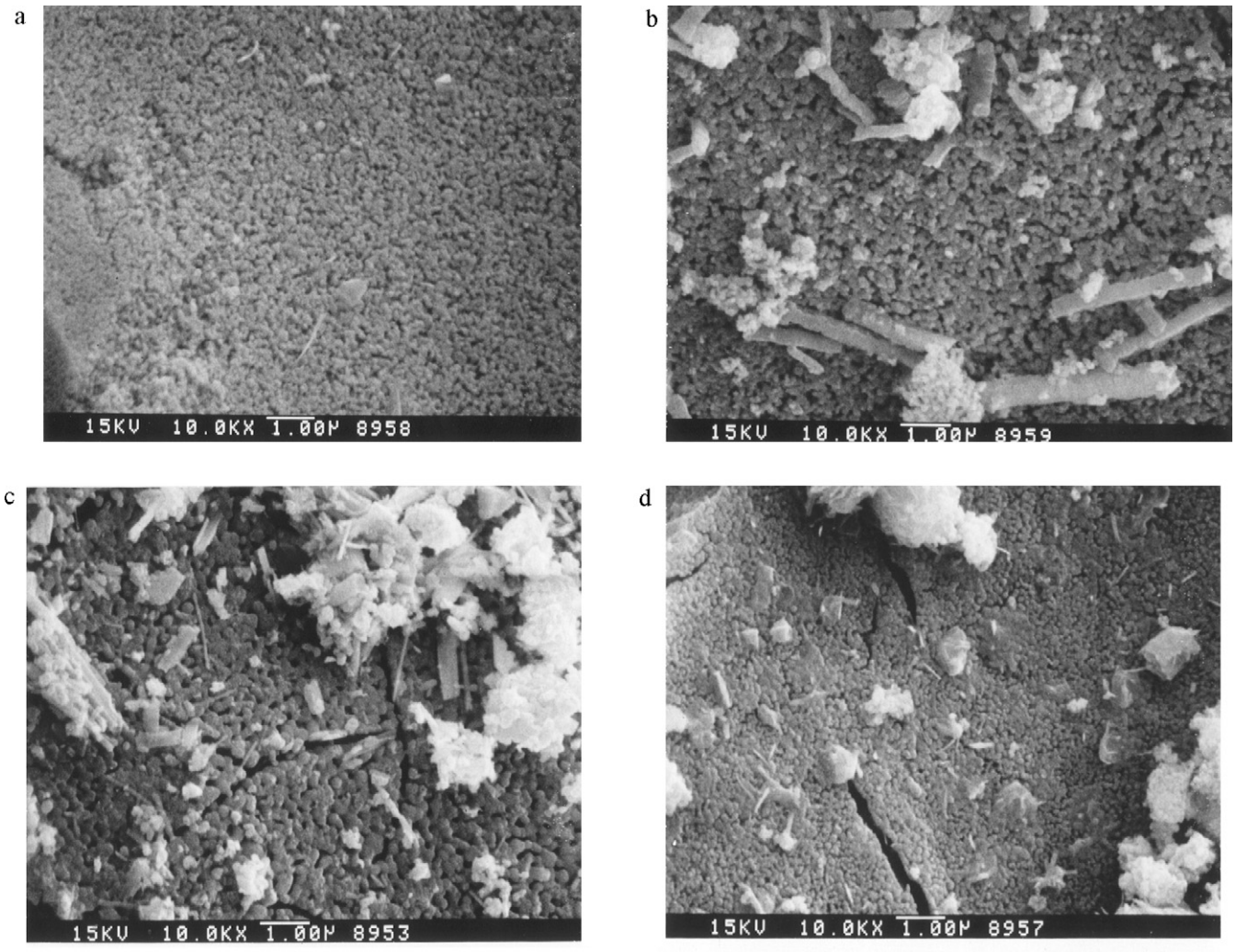

Fig. 4. Scanning electron micrographs of (a) fresh Sm–V–Sb catalyst, (b) used Sm–V–Sb catalyst, (c) used La–V–Sb catalyst, and (d) used Y–V–Sb catalyst.

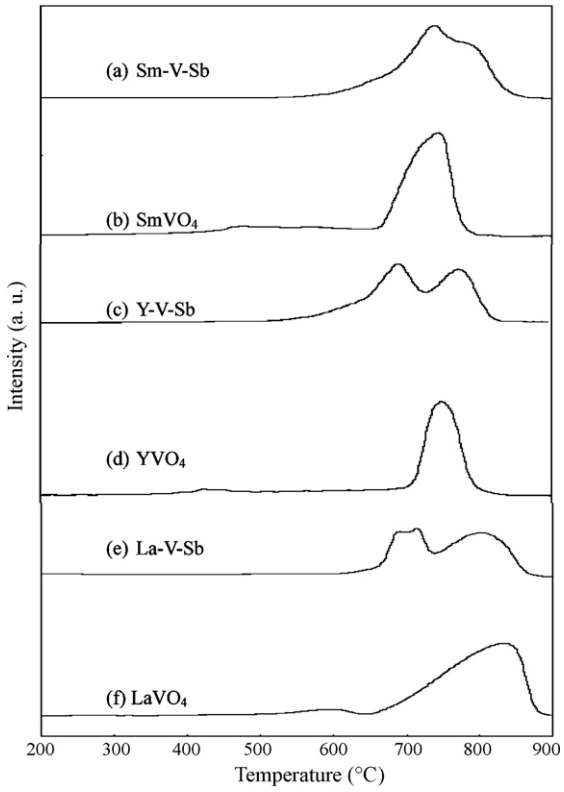

Fig. 5. TPR profiles of (a) Sm–V–Sb sample, (b) $SmVO_4$ sample, (c) Y–V–Sb sample, (d) YVO_4 sample, (e) La–V–Sb sample, (f) $LaVO_4$ sample.

3.3. SEM results

The results of scanning electron microscopic investigation are shown in Fig. 4 for the fresh Sm–V–Sb catalyst (graph a), the used Sm–V–Sb catalyst (graph b), the used La–V–Sb catalyst (graph c), and Y–V–Sb catalyst (graph d). The phase structure of all the R_E–V–Sb catalyst was a discrete tiny particle form. For all the R_E–V–Sb catalysts, the morphology of the used catalyst was similar to that of the fresh catalyst (e.g., graph (b) is similar to graph (a) for Sm–V–Sb catalyst), indicating that the catalysts were stable during reaction. Fig. 4(b)–(d) shows that white color particles appeared on the used catalyst surface, which should be the condensed sulfur products. The condensed sulfur particles might cause the intensity differences of catalyst XRD patterns (shown in Fig. 3) before and after catalytic test.

3.4. Temperature-programmed reduction studies

R_E–V–Sb catalyst reducibility was measured using a temperature-programmed reduction (TPR) method with hydrogen as the reductant. Fig. 5(a) and (b) shows the reduction profiles for Sm–V–Sb and $SmVO_4$. Fig. 5(c) and (d) shows the reduction profiles for Y–V–Sb and YVO_4. Fig. 5(e) and (f) shows the reduction profiles for La–V–Sb and $LaVO_4$.

The TPR profile for $SmVO_4$ (profile 5(b)) exhibits a single major reduction peak with peak temperature at around 750 °C, which is similar to the $SmVO_4$ reduction curve (a single peak with the maximum at 760 °C) observed by Barbero and Cadus [24]. The single reduction peak should be due to the reduction of Sm–O–V (i.e., the reduction of VO_4^{3-} tetrahedrons in $SmVO_4$). The TPR profile for YVO_4 (profile 5(d)) is similar to the YVO_4 reduction curve observed by Li and Chi [8]. It was proposed that bulk R_EVO_4 consists of R_EO_6 octahedral connected to VO_4 tetrahedra through V–O–R_E bonds. The oxidation states in R_EVO_4 are R_E^{3+} and V^{5+} [25]. The major reduction peak in profiles 5(b), 5(d) and 5(f) should be due to the reduction of R_E–O–V (i.e., the reduction of VO_4^{3-} tetrahedrons in R_EVO_4). There are small reduction plateaus in the reduction profiles of $SmVO_4$/YVO_4 (profiles 5(b) and 5(d)), and a small peak in the reduction profile of $LaVO_4$ (profile 5(f)), which might also due to the reduction of the residual V–O–V.

TPR profile Sm–V–Sb (profile 5(a)) exhibits a peak (at 740 °C) and a shoulder (at 800 °C), TPR profile Y–V–Sb (profile 5(c)) exhibits two distinct peaks (peak maxima occurs at 690 and 775 °C), TPR profile La–V–Sb (profile 5(e)) exhibits two distinct peaks (peak maxima occurs at 700 and 800 °C) and a shoulder (at 675 °C). TPR profile La–V–Sb sample is approximately the superimposition of the TPR curves of the corresponding $LaVO_4$ and $SbVO_4$ because TPR spectrum of $SbVO_4$ had two distinct peaks at 600 and 760 °C [21]. Profiles 5(b) and 5(d) show that TPR profile of $SmVO_4$ is similar to that of YVO_4, however, TPR profile of Sm–V–Sb (profile 5(a)) is significantly different from that of Y–V–Sb (profile 5(c)). The small residual V–O–V reduction peaks observed in R_EVO_4 TPR profiles (profile 5(b), 5(d) and 5(f)) disappeared in R_E–V–Sb TPR profiles (profiles 5(a), 5(c) and 5(e)), indicating that all the residual V–O–V were converted to Sb–O–V with the addition of antimony into R_EVO_4 catalysts.

Comparing the specific catalytic activity, Table 2 shows that the areal reaction rates (at 180 °C) of Sm–V–Sb and Y–V–Sb were 50 and 15.3 times those of $SmVO_4$ and YVO_4, respectively. The results indicate that $SbVO_4$ was much more active than R_EVO_4, and $SbVO_4$ (a crystalline material) should be the major species responsible for H_2S oxidation on R_E–V–Sb catalysts. It is known that $SbVO_4$ contained antimony in the oxidized state (Sb^{5+}) and vanadium in the reduced state. Our previous X-ray photoelectron spectroscopic data on $SbVO_4$ [20] indicate that both surface vanadium sites and surface antimony sites were in the reduced state after the oxidation of hydrogen sulfide.

It is known that TPR profiles depend strongly on the reductant used. Casagrande et al. [26] found that NH_3–TPR peak temperature was 330 °C lower than H_2–TPR peak temperature for a TiO_2 supported V_2O_5 catalyst, probably due to the fact that N–H bond is weaker than H–H bond. The bond strength of H–S is also weaker than H–H bond and it was proposed that proton transfer from H_2S to O_2^- had a small or negligible energy barrier [27]. Therefore, the temperature needed for catalyst reduction by H_2S (shown in Fig. 1) is much lower than the temperature needed for catalyst reduction by H_2 (shown in Fig. 5).

4. Conclusions

Three R_E–V–Sb catalysts were prepared by solid-state reaction between rare earth orthovanadate (with different R_E^{3+} ionic radii) and antimony oxide. The catalytic performances of R_EVO_4 in the selective oxidation of hydrogen sulfide to elemental sulfur were improved significantly with the addition of antimony oxide. For R_E–V–Sb catalysts, 'temperature window' width for obtaining 100% sulfur yield increased with increasing R_E^{3+} ionic radius. XRD and TPR results indicated that $SbVO_4$ was formed in the R_E–V–Sb catalysts. The synergy observed in the sulfur yield and selectivity with Sb addition was explained by the formation of $SbVO_4$ species and the improvement of site isolation effect. Among the three R_E–V–Sb catalysts, Sb addition had the greatest effect on the specific activity of Sm–V–Sb catalyst, which exhibited up to 50 times improvement on the areal rate compared to $SmVO_4$. The dramatic areal rate improvements of Sm–V–Sb and Y–V–Sb suggest that $SbVO_4$ was the active species for H_2S oxidation on R_E–V–Sb catalysts. In $SbVO_4$, Sb might be the active site for H_2S oxidation because vanadium is presented as the reduced state in $SbVO_4$.

Acknowledgment

The authors gratefully acknowledge the National Science Council of the Republic of China for financial support (Grant No. NSC-90-2214-E-029-002).

References

[1] M.P. Duncan, in: J.K. Kroschwitz, M. Howe-Grant (Eds.), Encyclopedia of Chemical Technology, vol. 23, Wiley, New York, 1997, p. 276.
[2] F. Janssen, in: F.J.J.G. Janssen, R.A. van Santen (Eds.), Environmental Catalysis, Imperial College Press, 2001 (Chapter 13).
[3] M. Capone, in: J.K. Kroschwitz, M. Howe-Grant (Eds.), Encyclopedia of Chemical Technology, vol. 23, Wiley, New York, 1997, p. 432.
[4] J.A. Lagas, J. Borsboom, P.H. Berben, Oil Gas J. 86 (1988) 68.
[5] R. Ketter, N. Liermann, Oil Gas J. 86 (1988) 63.
[6] E.V. Konshenko, A.V. Balaev, F.R. Ismagilov, S.I. Spivak, R.R. Safin, Chem. Tech. Fuels Oils 37 (2001) 212.
[7] H. Yasuda, in: S. Kobayashi (Ed.), Catalysis in Precision Polymerization, Wiley, Chichester, 1997, p. 189.
[8] K.T. Li, Z.H. Chi, Appl. Catal., A 206 (2001) 197.
[9] P. Courty, H. Ajot, C. Marcilly, B. Delmon, Powder Technol. 7 (1973) 21.
[10] C.T. Au, W.D. Zhang, H.L. Wan, Catal. Lett. 37 (1996) 241.
[11] R.K. Grasselli, in: G. Ertl, H. Knoezinger, J. Weitkamp (Eds.), Handbook of Heterogeneous Catalysis, vol. 5, Wiley, New York, 1997, p. 2302.
[12] B. Wu, M. Zinkevich, F. Aldinger, D. Wen, L. Chen, J. Solid State Chem. 180 (2007) 3280.
[13] E. Jungst, W. Nehb, in: G. Ertl, H. Knozinger, F. Schuth, J. Weitkamp (Eds.), Handbook of Heterogeneous Catalysis, vol. 5, Wiley-VCH, Weinheim, 2008, p. 4 (Chapter 12).
[14] B. Meyers, Chem. Rev. 76 (1976) 367.
[15] G. Wulfsberg, Inorganic Chemistry, University Science Press, Sausalito, CA, 2000.
[16] A. Martin, U. Bentrup, G. Wolf, Appl. Catal. A: Gen. 227 (2002) 131.
[17] R. Grabowski, B. Grzybowska, A. Kozlowska, J. Stoczynski, K. Wcisto, Y. Barbaux, Top. Catal. 3 (1996) 277.
[18] W.O. Milligan, L.M. Watt, H.H. Rachford, J. Phys. Colloid Chem. 53 (1949) 227.
[19] W. Fan, X. Song, S. Sun, X. Zhao, J. Solid Chem. 180 (2007) 284.
[20] K.T. Li, N.S. Shyu, Ind. Eng. Chem. Res. 36 (1997) 1480.
[21] K.T. Li, C.H. Huang, Eng. Chem. Res. 45 (2006) 7096.
[22] R.K. Grasselli, Catal. Today 49 (1999) 141.
[23] G. Centi, S. Perathoner, Appl. Catal. A: Gen. 124 (1995) 317.
[24] B.P. Barbero, L.E. Cadus, Appl. Catal. A: Gen. 252 (2003) 133.
[25] R.F. Reidy, K.E. Swider, J. Am. Ceram. Soc. 78 (1995) 1121.
[26] L. Casagrande, L. Lietti, I. Nova, P. Forzatti, A. Baiker, Appl. Catal., B 22 (1999) 63.
[27] A.J. Bell, T.G. Wright, J. Phys. Chem. A 108 (2004) 10486.